International Society for Rock Mechanics and Rock Engineering
Norwegian Group for Rock Mechanics

ISRM International Symposium
Eurock 2025 – Expanding the Underground Space
Trondheim, Norway, 16-20 June
ISBN 978-82-8208-079-8

Tension-torsion coupling effect and failure mechanism of anchoring section of anchor cable

Shuren Wang
School of Civil Engineering, Henan Polytechnic University, Jiaozuo, China
shurenwang@hpu.edu.cn (email of corresponding author)

Wenbing Guo
School of Energy Science and Engineering, Henan Polytechnic University, Jiaozuo, China

Abstract

For the anchor cable is a space spiral structure, there is reverse torque when it is pulled, and the existence of torque will reduce the axial tension and affect its anchoring performance. By using the self-developed cable tension-torsion coupling test system, three kinds of anchor cables with different diameters (9.5 mm, 12.7 mm, and 15.2 mm) commonly used in mining engineering were taken as the research materials, and the methods of indoor pull-out test, theoretical analysis and numerical simulation were adopted to study the coupling effect of tension and reverse torque of the anchor cable and the failure evolution process of the coupling force transfer of the anchor cable. Results show that the empirical formulas for calculating the torque of different diameters of anchor cables are fitted based on the torque-tension curve and the formula for calculating cable tension considering the decoupling of tension and reverse torque is presented based on the principle of work-energy. The expression of tension and torque of anchor cable is derived and the theoretical derivation is compared with the experimental results, and the accuracy of the mechanical model is verified. The equivalent stress, axial stress, shear stress and equivalent plastic strain of the section surface of the anchor cable under the condition of un- and free-rotation are analyzed by using numerical simulation. The tension-torsion coupling computational model of anchor cable is constructed to explain the failure evolution process of the anchoring system under the tension-torsion coupling effect. The axial tension and torque exhibit a cubic polynomial relationship in the first stage, which then transitions to a linear relationship as the conditions change. The results obtained can provide a solid foundation for tensile force analysis and anchorage force design of anchor cables.

Keywords

Anchor cable, Pull-out test, Tension-torsion coupling, Mechanical model, Failure mechanism

ISRM

NBG

1 Introduction

Anchor cable anchoring technology is a highly effective means of controlling deformation and stabilizing engineering rock and soil masses (Li et al. 2017; Li et al. 2022; Shi et al. 2024). This technology offers significant benefits, including active support, enhanced security, and economic efficiency, which have led to its widespread application in various engineering fields globally. While rock bolt and anchor cable anchoring technologies share similarities in load transfer mechanisms, the anchor cable produces a torque perpendicular to its section during the pulling process, causing the cable strands to rotate reversely (Wang 2015). Pull-out tests have shown that if the anchor cable rotates freely, the strands tend to slide along the original grooves of the anchoring resin, resulting in a torsional stress state. Conversely, if the rotation is constrained, the anchoring resin experiences both axial pull-out load and shear force, leading to complex stress states (Andrianov et al. 2020).

Over the years, several mechanical models have been developed to understand the behavior of anchor cables, including bond strength, axial force and torque, and shear models of structural planes. Early models, such as the one proposed by Kaiser et al. (1992), simplified the stranded cable structure and considered radial displacement and lateral confining pressure. Hyett et al. (1995) proposed a model that accounted for torque generated by the pull-out load, but it simplified torque as an equivalent axial force component, which did not align with actual conditions. The elastic bond model, proposed by Farmer (1975), theoretically deduced and experimentally verified that the axial force of the cable attenuates exponentially along the axial direction. Recent research has deduced analytical expressions for the axial force of the anchor cable, shear force of the structural plane, and displacement of the anchorage element, assuming a three-stage line for the shear stress-strain curve of the structural plane (Li and Stillborg 1999; Cai and Champaigne 2012; Cao et al. 2014). Chinese scholars have primarily focused on the bond-slip constitutive relationship between steel reinforcement and concrete (Wang et al. 2017; Lin et al. 2019). Considering the heterogeneity and nonlinear failure properties of rock and soil masses, analytic formulas for load transfer in the anchorage segment have been deduced, and the coupling effect of the anchorage system has been verified (Zhang and Chen 2015; Li et al. 2021; Pytlik and Szot 2023). However, these studies often simplify theoretical formulas and largely ignore the unwinding effect of torque during the pulling process of the anchor cable.

The anchor cable, characterized by its spatial spiral structure, exhibits a torque perpendicular to its section upon stretching. This torque induces reverse rotation in each strand, reducing axial tension and exerting a notable influence on the evaluation of its bearing capacity. Regrettably, contemporary anchoring design theories overlook this torque unwinding effect, resulting in designs that fall short of engineering standards. Ongoing research endeavors concerning anchor cable bearing mechanisms, design theories, and calculation methodologies remain incomplete, emphasizing the urgency for a more profound comprehension of mechanical transmission, failure modes, and interface interactions. Therefore, it is of utmost importance to delve into the failure mechanism of the anchoring section of tension-torsion coupled anchor cables, taking into account structural attributes, interactions with anchoring media, and coupling dynamics with the surrounding rock. Such research will furnish engineers with invaluable insights, enabling them to formulate precise prediction models, design dependable and efficient anchoring systems, minimize costs and maintenance requirements, and augment structural safety. Furthermore, it will fortify and refine existing anchoring theories of anchor cables, contributing significantly both theoretically and practically.

2 Materials and methods

2.1 Test materials and loading equipment

The test anchor cables, which were produced by Tianjin Ruitong Limited Company and consisted of 1 × 7 steel strands, were manufactured from high-carbon steel wire rod through processes of cold drawing and twisting. These anchor cables were available in three diameters: 9.5 mm, 12.7 mm, and 15.2 mm, and each diameter was offered in three lengths: 850 mm, 1150 mm, and 1350 mm. During axial tensile experiments, these anchor cables were used with locking lengths of 500 mm, 750 mm, and 1000 mm, respectively. The specification parameters of the anchor cables with varying diameters are outlined in Table 1.

Table 1 Main parameters of the anchor cables.

Structure	Diameter (mm)	Cross-section area (mm^2)	Maximum load (kN)	Unit weight (kg/m)
1×7 Standard type	9.5	54.8	102	0.430
	12.7	98.7	184	0.775
	15.2	140.0	260	1.101

The LW-1000 self-developed equipment, which was utilized in the test (Wang et al., 2020a), comprises a loading device, a measuring device, and a data acquisition and processing system (Fig. 1). This equipment facilitates real-time data collection, instant display, and real-time chart plotting. The components of the equipment are labeled as follows: 1-Pedestal, 2-Cylinder body, 3-Lower beam, 4-Upper beam, 5-Piston rod, 6-Torque sensor, 7-Positioning pin, 8-Stretch rotating shaft, 9-Trolley track, 10-Carriage, 11-Anchor cable, and 12-Concrete columns.

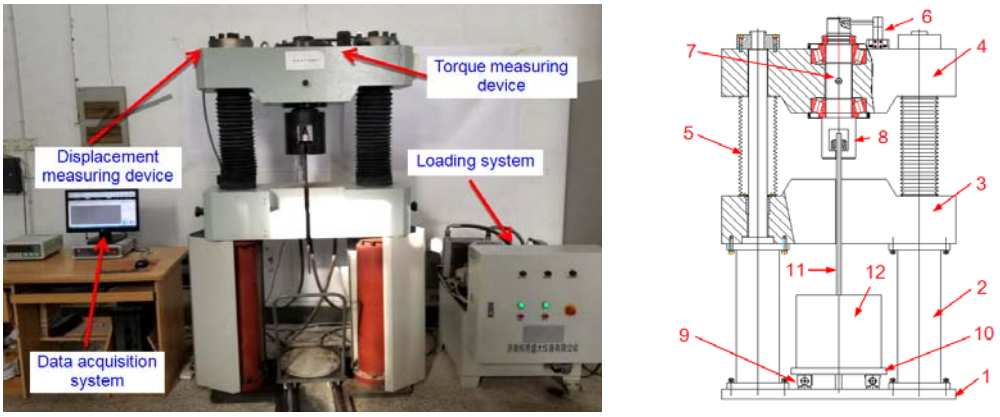

(a) Test equipment diagram (b) Structural diagram

Fig. 1 The loading and measurement device.

2.2 Computational model and calculation parameters

The three-dimension model of the steel strand was established by Abaqus (Wang et al. 2020b). The mesh division of the model is shown in Fig. 2. The material parameters of steel strand are measured according to the tensile test of steel wire. The constitutive parameters after transformation are shown in Table 2.

(a) Computational model (b) Cross-section of the model

Fig. 2 Computational model and its meshes of cable-bolts.

Table 2 Material parameters of steel strand.

Elastic modulus (GPa)	Poisson's ratio	Density (t/m^3)	Yield/Tensile strength (MPa)	Plastic strain
210	0.30	7.85	1810/2020	0.05

2.3 Sample design and preparation

As illustrated in Figs. 3 and 4, the central pulling specimen was employed in the test (Wang et al., 2020c; Wang et al., 2021). The anchor cable was anchored at the central section of the cylindrical concrete specimen, with the anchorage segment positioned at the middle to upper portion along the central axis of the cylinder. A total of six groups of specimens were prepared for the test, with each group comprising three specimens. By varying the confining pressure (0, 2.5, and 5.0 MPa) and the constraint conditions at the top of the anchor cable (non-rotation versus free rotation), the study

investigated the impact of each factor on the failure mode, ultimate bearing capacity, and load-deformation curve of the internal anchorage segment.

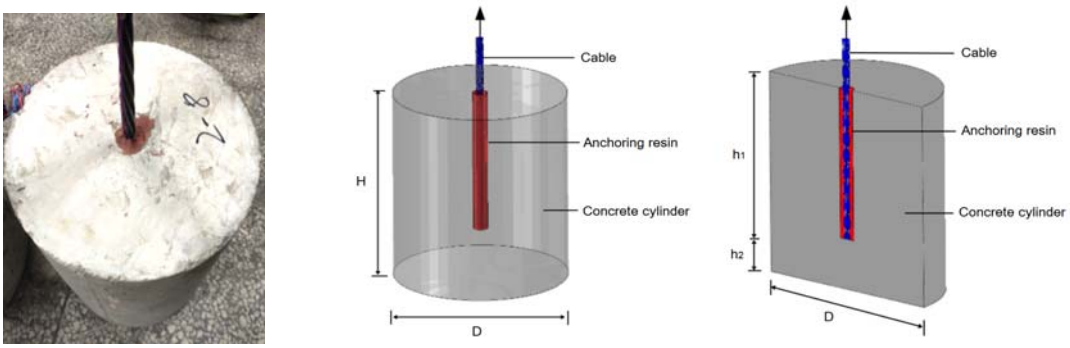

(a) Sample photo (b) Schematic diagram (c) Semi-cylindrical diagram

Fig. 3 Samples of pull-out test.

3 Results analysis and discussion

3.1 Characteristics analysis of Tension-displacement-torque curves

Since the locking length has minimal impact on torque and tension, the typical axial force-displacement-torque curves for anchor cables with a 12.7 mm diameter and a locking length of 500 mm are depicted in Fig. 4(a). The displacement shown in Fig. 4 encompasses not only the tensile displacement of the steel strand but also the sliding displacement between the steel strand and the clamp.

Observing Fig. 4(a), we can see that the axial force-displacement-torque curves of the anchor cables exhibit three stages: Stage 1 (pre-tensioning stage), Stage 2 (elastic stage), and Stage 3 (plastic stage). Based on experimental data, an empirical formula for the torque of anchor cables has been fitted (R^2=0.99), and the torque expressions for anchor cables of varying diameters are provided below:

$$M = cP\mathrm{d} = \left(0.025 + 7.045\times10^{-5} e^{0.318d}\right)Pd \tag{1}$$

Where M Torque of anchor cable, N·m;
P Axial force of anchor cable, kN;
c Torque coefficient;
d Anchor diameter, mm.

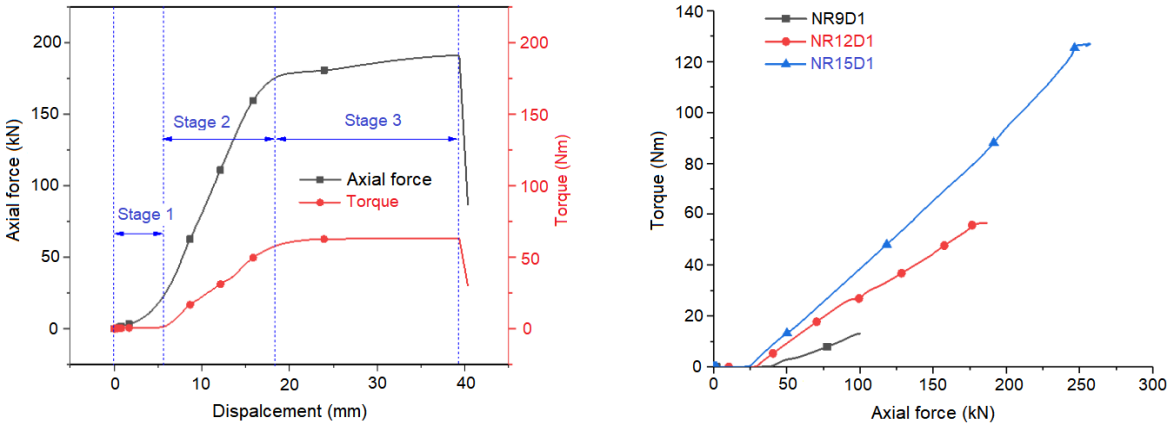

(a) 12.7 mm anchor cable (b) Axial force-torque curves

Fig. 4 Axial force-displacement-torque typical curves and axial force-torque curves of different diameter cables.

3.2 Decoupling analysis of axial tensile force and torgue

When the anchor cable is under free rotation condition, its torque is released, and consequently, part of the work done by the pulling force is utilized for reverse rotation, disregarding friction and other

factors. The work resulting from the rotation of the anchor cable is equivalent to the work done by a hypothetical reverse rotation force ΔF in causing tensile displacement. Based on the work-energy principle:

$$W_1 - W_2 = \frac{\Delta FS}{2} \tag{2}$$

According to Eq. (2), the tension-torque coupling formula is proposed as follows:

$$\eta = \frac{\Delta F}{F} = \frac{2(W_1 - W_2)}{FS} \tag{3}$$

Where W_1 Work of the anchor cable performed under free rotation condition, J;
W_2 Work of the anchor cable performed under non-rotating condition, J;
ΔF Reverse rotation force, kN;
S Displacement, mm;
η Axial force-torque coupling coefficient.

Based on the experimental data, the tensile-torque coupling coefficients for anchor cables with diameters of 9.5 mm, 12.7 mm, and 15.2 mm have been calculated, yielding ratios of 9%, 10%, and 12%, respectively.

In general, the axial force-displacement curves derived from both experimental tests and numerical analyses exhibit good agreement. However, there is a noticeable discrepancy in the displacement during the elastic phase. This inconsistency is primarily attributed to the pretension stage in the experimental setup, which introduces nonlinear loading behavior in the initial stages, whereas the numerical simulation assumes linear loading. Despite this difference, the rotational behavior, whether under free rotation or non-rotation conditions, remains consistent in both tests and simulations, with a decrease in stiffness observed under free rotation conditions.

3.3 Cross-section stress analysis of anchor cable

3.3.1 Equivalent stress analysis of anchor cable

We used the equivalent stress method to analyze the comprehensive stress state of the anchor cable. Since the stress distributions of the three diameters were similar, the 15.2 mm cable was taken as an example to analyze the tension-torsion coupling characteristics. When the strain in the elastic phase reached 0.64%, the equivalent stress distribution across the section of the anchor cable under conditions of restricted and free rotations is shown in Fig. 5. As seen from Fig. 5, the restricted rotation shows highest stress at wire contacts, followed by center wire, with outer wire stress lowest. Contact pressure causes local stress concentration with minimal overall impact. Central wire stress is uniform, while outer wire stress decreases outward in layers. Under free rotation, highest stress is still at wire contacts, with torsion causing stress concentration. Central wire stress decreases concentrically outward, while outer wire stress decreases in a half-moon pattern, showing delamination.

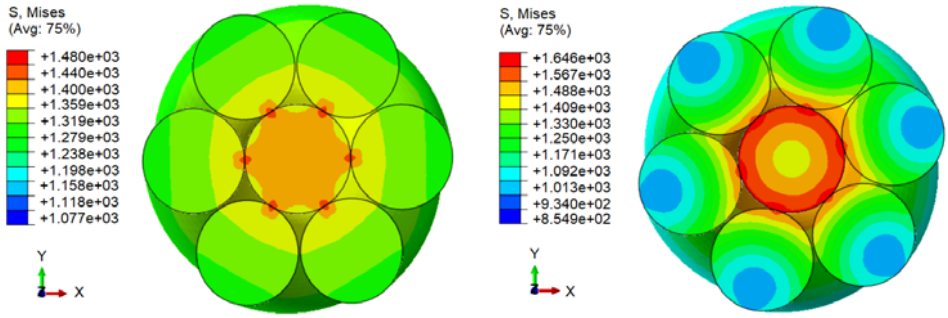

(a) Restricted rotation (b) Free rotation

Fig. 5 Equivalent stress of 15.2 mm diameter anchor cable under two conditions (MPa).

3.3.2 Axial stress analysis of tension-torsion coupling effects of anchor cable

At a strain of 0.64%, Fig. 6 shows the axial stress distribution across the anchor cable's cross-section under restricted and free rotation conditions. Without rotation, the stress is relatively uniform, with low concentrations at contact points due to combined tensile and compressive forces. The inner wire

bears the highest stress, while outer wires' stress decreases gradually with minimal fluctuation. Under free rotation, however, stress distribution becomes irregular, with the inner wire experiencing notably higher stress and outer wires showing a clear layering effect.

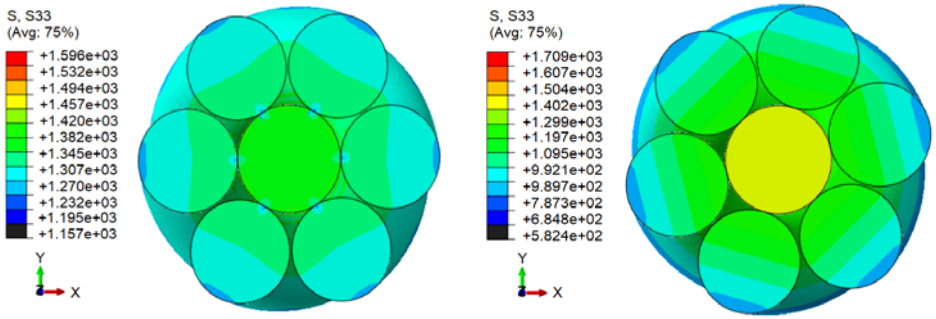

(a) Restricted rotation (b) Free rotation

Fig. 6 The cross-section axial stress under two conditions.

3.3.3 Shear stress analysis of tension-torsion coupling effects of anchor cable

As seen in Fig. 7: Under restricted rotation, the inner wire exhibits positive shear stress (indicating an untwisting direction) that is nearly zero, suggesting no twisting occurs. The outer wire, on the other hand, experiences negative shear stress (indicating a tightening direction) due to the counter torque. In the case of free rotation, the cross-sectional shear stress distribution takes on a petal-like form. The contact areas between the inner and outer wires show close values but opposite directions in shear stress, indicating that the inner wire is also twisted by the shear effect of the outer wire. The internal and external torques cancel each other out. The shear stress in the central wire decreases concentrically from the outer layer towards the inside. Meanwhile, the shear stress in the outer wire gradually transitions from negative to positive, with a critical layer located in the middle of the anchor cable.

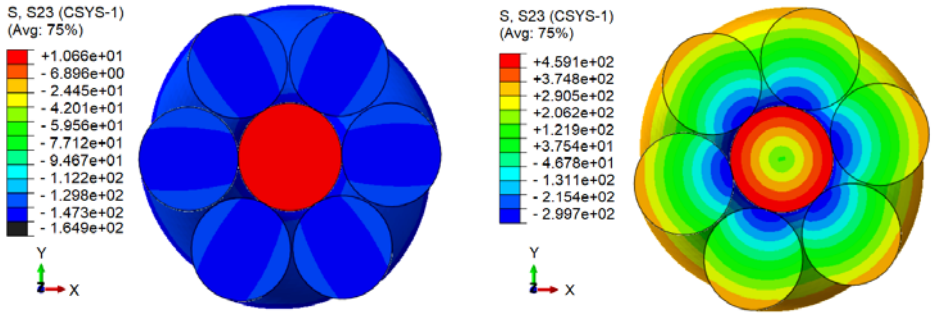

(a) Restricted rotation (b) Free rotation

Fig. 7 The cross-section shear stress under two conditions.

3.4 Constitutive relation of anchorage segment

As seen in Fig. 8(a), during the pull-out test under loading conditions, the free end of the anchor cable generates a torque perpendicular to its cross-section. The load-torque-displacement curve comprises three characteristic stages: the loading stage, the softening stage, and the residual stage. Based on the experimental results, a theoretical model of the pull-out load-torque-displacement constitutive relationship prior to residual failure was proposed.

The relationship curve is termed the YHW-FISH model, as illustrated in Fig. 8(b). The model encompasses two stages: the loading stage and the softening stage. Since both stages exhibit non-linear characteristics, the functional relationships of the YHW-FISH model can be described by Eqs. (3) and (4).

Loading stage:

$$F = 171.07 - \frac{33572.75}{4(x-1.22)^2 + 196.56} \qquad (0 < x < x_1) \qquad (3)$$

$$T = -2.74 \times 10^{-3} x^3 + 0.26x^2 - 7.44x + 11.36$$

Softening stage:

$$F = 40.76 + \frac{5891.25}{x} e^{-1.39\left[\ln\frac{x}{52.88}\right]^2} \qquad (x_1 < x < x_2) \qquad (4)$$

$$T = 1.26\times10^{-2}x^2 + 4.4x - 205.85$$

Where F Pull-out load, kN;
T Torque, Nm;
x The corresponding slip, mm;
x_1 The dividing line between the loading stage and the softening stageorque, mm;
x_2 The dividing line of the softening stage and the residual stage, mm.

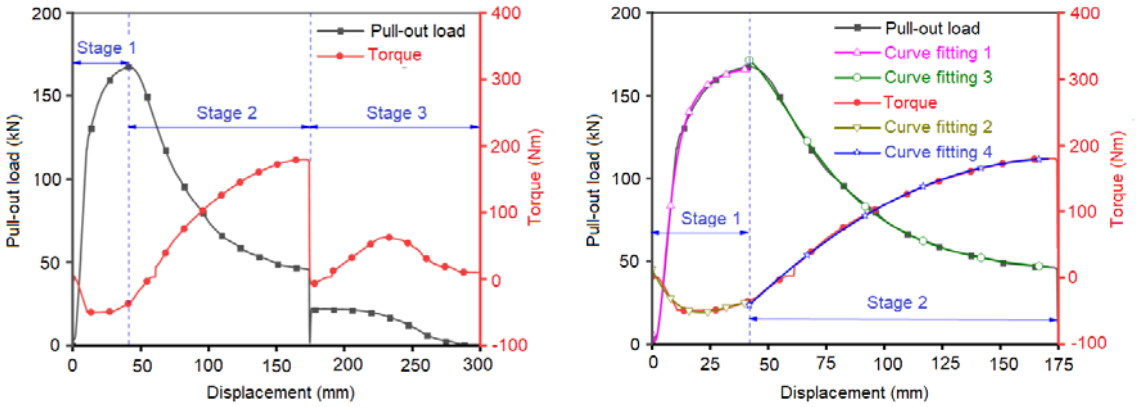

(a) The pull-out load-torque-displacement curves (b) The fitting curves

Fig. 8 The pull-out load-torque-displacement curves and the fitting curves.

Based on the above analysis, the failure mechanism of the anchorage segment of the anchor cable can be determined: pull-out failure and shear failure are the main causes of failure in the anchorage segment. However, pull-out failure and shear failure do not occur synchronously; the failure mechanism of the anchorage segment involves pull-out first, followed by shear failure. During the loading phase of the pull-out test, it primarily exhibits pull-out failure, with shear failure becoming dominant after the pull-out load gradually reaches its peak value.

4 Conclusions

Based on the structural characteristics of the anchor cable, the coupling effect of tension and torsional moment, along with the failure load mechanism of the anchor section, was analyzed through a combination of laboratory tests, numerical simulations, and theoretical analyses. The main conclusions obtained are as follows:

A formula for calculating cable tension, which considers the decoupling of tension and inverse torque, has been derived based on functional principles. The expressions for cable tension and torque have been derived and experimentally validated. The maximum equivalent stress in the cable section occurs at the contact area between the inner and outer wires, and this stress is found to be greater under conditions of free rotation compared to restricted rotation.

The relationship between the torque of the anchor cable and the pulling load can be characterized by two distinct stages. In the loading stage, the torque increases with the pulling load until a peak value is reached, followed by a decrease. This relationship is accurately described by a cubic polynomial. In the softening stage, the torque increases linearly as the pulling load decreases.

In this study, a comprehensive load-torque-displacement coupling relationship for the anchor cable has been established, providing a solid theoretical basis and technical support for engineering practice. Future research should focus on further refining evaluation methods for load transfer characteristics and developing advanced failure prediction techniques for anchoring systems.

References

Andrianov IV, Danishevskyy VV, Topol H. (2020) Local stress distribution in composites for pulled-out fifibers with axially varying bonding. Acta Mechanica 231(5): 2065-2083. DOI: 10.1007/s00707-020-02634-6

Cai M, Champaigne D. (2012) Influence of bolt-grout bonding on MCB cone bolt performance. International Journal of Rock Mechanics and Mining Sciences 49: 165-175. DOI: 10.1016/j.ijrmms.2011.11.006

Cao C, Ren T, Cook C, Cao YJ. (2014) Analytical approach in optimising selection of rebar bolts in preventing rock bolting failure. International Journal of Rock Mechanics and Mining Sciences 72: 16-25. DOI: 10.1016/j.ijrmms.2014.04.026

Farmer IW. (1975) Stress distribution along a resin grouted rock anchor. International Journal of Rock Mechanics and Mining Sciences 12(11): 347-351. DOI: 10.1016/0148-9062(75)90168-0

Hyett AJ, Bawden WF, Macsporran GR, Moosavi M. (1995) Constitutive law for bond failure of fully-grouted cable bolts using a modified Hoek cell. International Journal of Rock Mechanics and Mining Sciences & Geomechanics Abstracts 32(1): 11. DOI: 10.1016/0148-9062(94)00018-X

Li C, Stillborg B. (1999) Analytical models for rock bolts. International Journal of Rock Mechanics and Mining Sciences 36(8): 1013-1029. DOI: 10.1016/S1365-1609(99)00064-7

Li DQ, Cai M, Masoumi H. (2021) A constitutive model for modified cable bolts exhibiting cone shaped failure mode. International Journal of Rock Mechanics and Mining Sciences 145: 104855. DOI: 10.1016/j.ijrmms.2021.104855

Li X, Si GY, Oh J, Corbett P, Xiang ZZ, Aziz N, Mirzaghorbanali A. (2022) Effect of pretension on the performance of cable bolts and its optimisation in underground coal mines with various geological conditions. International Journal of Rock Mechanics and Mining Sciences 152: 105076. DOI: 10.1016/j.ijrmms.2022.105076

Li XW, Aziz N, Mirzaghorbanali A, Nemcik J. (2017) Comparison of the shear test results of a cable bolt on three laboratory test apparatuses. Tunnelling and Underground Space Technology 61: 82-89. DOI: 10.1016/j.tust.2016.10.003

Lin HW, Zhao YX, Ozbolt J, Feng P, Jiang C, Eligehausen R. (2019) Analytical model for the bond stress-slip relationship of deformed bars in normal strength concrete. Construction and Building Materials 198: 570-586. DOI: 10.1016/j.conbuildmat.2018.11.258

Kaiser PK, Yazici S, Nosé J. (1992) Effect of stress change on the bond strength of fully grouted cables. International Journal of Rock Mechanics and Mining Sciences & Geomechanics Abstracts 29(3): 293-306. DOI: 10.1016/0148-9062(92)93662-4

Shi GC, Yang XJ, Sun JH, Tao ZG, Sousa LRE. (2024) Experimental study on the control characteristics of the negative Poisson's ratio structural anchor cable on the large deformation of rainfall-induced landslide. Bulletin of Engineering Geology and the Environment 83(4): 134. DOI: 10.1007/s10064-024-03641-w

Wang CH. (2015) Some end effects in a cylindrically orthotropic circular tube of finite length with radial inhomogeneity subjected to torsional loads. Acta Mechanica 226(6): 1707-1723. DOI: 10.1007/s00707-014-1283-1

Pytlik A, Szot M. (2023) Comparative testing of cable bolt and wire rope lacing resistance to static and dynamic loads. Archives of Mining Sciences 68(4): 707-724. DOI: 10.24425/ams.2023.148158

Wang Q, Wei ZZ, Xu G, Xiang J, Pan Q. (2017) Bond-slip model for reinforced concrete under deicer-frost environment. Journal of Building Materials 20(5): 692-699. DOI: 10.3969/j.issn.1007-9629.2017.05.006

Wang SR, Wang YH, Gong J, Wang ZL, Huang QX, Kong FL. (2020a) Failure mechanism and constitutive relation for an anchorage segment of an anchor cable under pull-out loading. Acta Mechanica 231(8): 3305-3317. DOI: 10.1007/s00707-020-02717-4

Wang SR, Wang YH, Wang ZL, Gong J, Li CL. (2021) Anchoring performances analysis of tension-torsion grouted anchor cable under free and non-free rotation conditions. DYNA 96(2): 166-172. DOI: https://doi.org/10.6036/9985

Wang SR, Wang ZL, Chen YB, Wang YH, Huang QX. (2020b) Mechanical performances analysis of tension-torsion coupling anchor cable. International Journal of Simulation Modelling, 19(2): 231-242. DOI: 10.2507/IJSIMM19-2-512

Wang SR, Wang ZL, Gong J, Wang YH, Huang QX. (2020c). Coupling effect analysis of tension and reverse torque during axial tensile test of anchor cable. DYNA, 95(3): 288-293. DOI: 10.6036/9603

Zhang X, Chen SH. (2015) Analytical solution for load transfer along anchored section of prestressed anchor cable. Rock and Soil Mechanics 36(6): 1667-1675. DOI: 10.16285/j.rsm.2015.06.019